


Article

Improvement of Alkali Metal Resistance for NH₃-SCR Catalyst Cu/SSZ-13: Tune the Crystal Size

Zexiang Chen ¹ , Meiqing Shen ^{1,2}, Chen Wang ^{1,3}, Jianqiang Wang ¹, Jun Wang ^{1,*} and Gurong Shen ^{4,*}

¹ School of Chemical Engineering & Technology, Tianjin University, Tianjin 300072, China; tjucz@tju.edu.cn (Z.C.); mqshen@tju.edu.cn (M.S.); chenwang87@tju.edu.cn (C.W.); jianqiangwang@tju.edu.cn (J.W.)

² Collaborative Innovation Centre of Chemical Science and Engineering (Tianjin), Tianjin 300072, China

³ School of Environmental and Safety Engineering, North University of China, Taiyuan 030051, China

⁴ School of Materials Science and Engineering, Tianjin University, Tianjin 300350, China

* Correspondence: wangjun@tju.edu.cn (J.W.); gr_shen@tju.edu.cn (G.S.)

Abstract: To improve the alkali metal resistance of commercial catalyst Cu/SSZ-13 for ammonia selective catalytic reduction (NH₃-SCR) reaction, a simple method to synthesize Cu/SSZ-13 with a core-shell like structure was developed. Compared with smaller-sized counterparts, Cu/SSZ-13 with a crystal size of 2.3 μm exhibited excellent resistance to Na poisoning. To reveal the influence of the crystal size on Cu/SSZ-13, physical structure characterization (XRD, BET, SEM, NMR) and chemical acidic distribution (H₂-TPR, UV-Vis, Diethylamine-TPD, pyridine-DRIFTS, EDS) were investigated. It was found that the larger the crystal size of the molecular sieve, the more Cu is distributed in the crystal core, and the less likely it was to be replaced by Na to generate CuO. Therefore, a 2.3 μm sized Cu/SSZ-13 well-controlled the reactivity of the side reaction NH₃ oxidation and the generation of N₂O. The result was helpful to guide the extension of the service life of Cu/SSZ-13.

Keywords: alkali metal poison; Cu/SSZ-13; crystal size; NH₃-SCR



Citation: Chen, Z.; Shen, M.; Wang, C.; Wang, J.; Wang, J.; Shen, G.

Improvement of Alkali Metal Resistance for NH₃-SCR Catalyst Cu/SSZ-13: Tune the Crystal Size. *Catalysts* **2021**, *11*, 979. <https://doi.org/10.3390/catal11080979>

Academic Editor: Anker Degn Jensen

Received: 21 July 2021

Accepted: 16 August 2021

Published: 16 August 2021

Publisher's Note: MDPI stays neutral with regard to jurisdictional claims in published maps and institutional affiliations.



Copyright: © 2021 by the authors. Licensee MDPI, Basel, Switzerland. This article is an open access article distributed under the terms and conditions of the Creative Commons Attribution (CC BY) license (<https://creativecommons.org/licenses/by/4.0/>).

1. Introduction

For health and environmental considerations, the current community strongly demands to improve air quality. Environmental protection agencies around the world have introduced more and more stringent motor vehicle exhaust emission regulations on CO, nitrogen oxides (NO_x), unburned hydrocarbons and particulate matter [1]. The commercial technology of pollutants elimination is to adopt efficient catalytic converters. Cu/SSZ-13 (SSZ-13 is one framework type code of chabazite zeolite), one of the most excellent NO_x removal catalysts, has been commercially used in the exhaust after-treatment system of medium and heavy diesel vehicles [2–6].

In the past decade, numerical theoretical and experimental studies have revealed the pore structure, NH₃-SCR catalytic active sites, high-temperature hydrothermal stability, sulfur poisoning mechanism and alkali metal poisoning mechanism of Cu/SSZ-13 [7–20]. Alkali metals, such as sodium (Na) and potassium (K) are present in conventional diesel fuel and biodiesel fuel, and have been implicated in internal injector deposits [21,22]. Besides, alkali metals also exist in automotive urea, such as diesel exhaust fluid (DEF) or AdBlue. Previous reports have shown that alkali metal ions are volatilized under high-temperature conditions and diffuse to the surface of the catalyst, causing the catalyst to be poisoned [23,24]. Fundamental researches have revealed the alkali metal poisoning mechanism of Cu/CHA catalysts [25,26]. Researchers suggest that alkali metal ions can destroy the active center Cu²⁺ and degrade the zeolite framework, causing irreversible deactivation. However, how to improve the tolerance of Cu/zeolite catalysts to alkali metals is rarely reported. Yan et al. reported that highly dispersed Cu₄AlO_x mixed oxides have a good alkali metal resistance [27]. However, the multiple Cu complex cannot fit in

the CHA's steric pore size and the inactive CuO clusters are easily formed in the CHA zeolites [28]. Du et al. compared the alkali resistance of conventional V_2O_5/WO_3-TiO_2 catalysts and Fe_2O_3/HY zeolite catalysts and found that the HY zeolites played an alkali-buffer role to retain the catalytic activity [29]. Zha et al. developed a hollandite Mn-Ti oxide promoted Cu-SAPO-34 (SAPO-34 is one framework type code of chabazite zeolite) catalysts (HMT@Cu-S). HMT layer can trap alkali metal ions to protect Cu/SAPO-34 [30]. The similarity of previous research lies in the use of outer shell materials to protect the inner structure. However, the synthesis of core-shell materials often requires fine control, and it is difficult to achieve industrial low-cost production. To meet industrial needs, we tried to develop a simple preparation process to obtain core-shell-like molecular sieves with good alkali metal resistance. In our previous study [31], it was found that different crystal sizes of the Cu/SAPO-34 can affect the spatial distribution of acid sites, which inspired us to adjust the acid sites on the outer surface of the molecular sieve by tuning the crystal size.

In this work, we report that Cu/SSZ-13 catalysts with different crystal sizes (0.4–2.3 μm) present distinct sodium metal ions resistance. Due to the similar deactivation effect of Na and K, we only choose Na to study the improvement of alkali metal resistance [25]. Na-poisoned Cu/SSZ-13 with crystal size of 2.3 μm showed much higher NH_3 -SCR activity than ones with a size of 0.4 μm . The distribution of acidity and Cu ions is characterized by H_2 -TPR, UV-vis, diethylamine-TPD, and pyridine-DRIFTs. By enlarging the crystal size of SSZ-13, the active center Cu ions are allowed to locate the subsurface or inner core, so that the outer layer of the zeolites buffer the foreign alkali metal poisoning. Adjusting the distribution of acid sites by modifying the crystal size provides a simple technical route to improve alkali metal poisoning.

2. Results and Discussions

The crystallization process of SSZ-13 zeolites is mainly divided into induction period and crystallization period [32]. During the induction period, the raw materials in the gel gradually gather to form crystal nuclei, and the crystal grows rapidly after entering the crystallization period. The crystal size of SSZ-13 can be affected by the crystallization time, crystallization temperature, gel pH and added amount of crystal seed. Through a series of trials, we found that the crystal size of SSZ-13 is most sensitive to the amount of seed crystal added. The as-prepared catalysts are visualized by SEM. As shown in Figure 1, the average crystal size of each sample is obtained based on the statistical results of ~ 100 grains. All samples present cubic shape and uniform particle size. The results show that the crystal sizes of the synthesized SSZ-13 are 0.4, 0.8, and 2.3 μm .

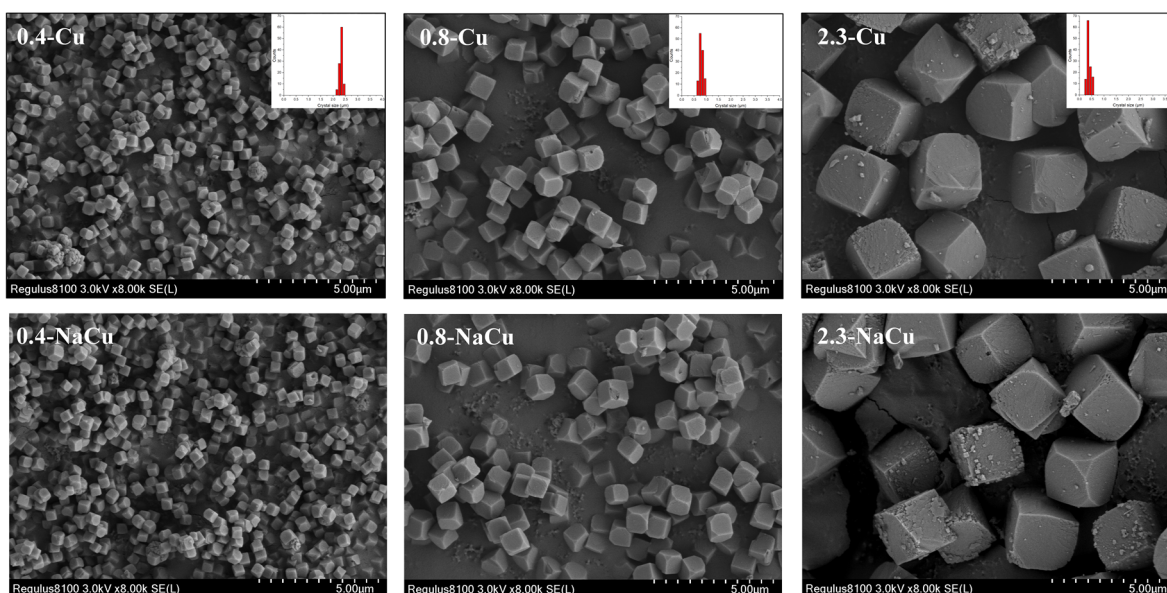


Figure 1. SEM images of Cu/SSZ-13 catalysts with different crystal sizes.

2.1. NH₃-SCR and NH₃ Oxidation Activity

Figure 2 presents the NH₃-SCR activity and side product N₂O concentration of catalysts before and after Na poisoning. Before Na poisoning, Cu/SSZ-13 with different crystal sizes present similar NH₃-SCR activities. It can be observed that between 350–400 °C, SCR activity increases with increasing crystal sizes. In this temperature range, the increasing temperature induces the active center Cu²⁺ to migrate from the solvated form (Cu^{II}(NH₃)_n(H₂O)_m) to the molecular sieve framework (Z₂Cu^{II} or ZCu^{II}OH) [33–35]. The change in reaction activity is mainly dominated by the number of isolated Cu ions. Such trend is consistent with the copper content in order: 2.3-Cu (1.44 wt %) > 0.8-Cu (1.38 wt %) > 0.4-Cu (1.05 wt %) (Table S1). Thereafter in the higher temperature region (>400 °C), all samples have decreased activities, which is caused by the side reaction NH₃ oxidation reaction. The NH₃ can be oxidized to N₂ by either NO_x or O₂. The competition between SCR reaction and NH₃ oxidation by O₂ at high temperatures (>350 °C) is widely reported [6]. The amount of N₂O produced at a concentration of less than 11 ppm in the entire temperature window indicates that the catalysts have good N₂ selectivity (Figure 2c). NO_x can be reduced to N₂O or N₂ by NH₃. Normally, 5–10 ppm of N₂O production for the state-of-the-art Cu-based catalysts is usually observed in the literature [2,3]. After Na poisoning (Figure 2b), the three samples show completely different NH₃-SCR reactivities, whose order is: 2.3-NaCu > 0.8-NaCu > 0.4-NaCu. The activity of 0.4-NaCu decreases most significantly, and the NO_x conversion drops sharply from 98% to 30% at ~300 °C. Figure 2d shows the N₂O generation curve with temperature ramping. Surprisingly, the maximum amount of N₂O produced by 0.4-NaCu (~75 ppm) at 280 °C is 3 times that of 0.8-NaCu (~25 ppm) and 7 times that of 2.3-NaCu (~10 ppm). The results show that the geometric size of the molecular sieve greatly affects the NH₃-SCR catalytic activity and N₂ selectivity of the Na-poisoned CuSSZ-13 catalysts. In short, the Cu/SSZ-13 catalyst with a larger crystal size has better Na resistance.

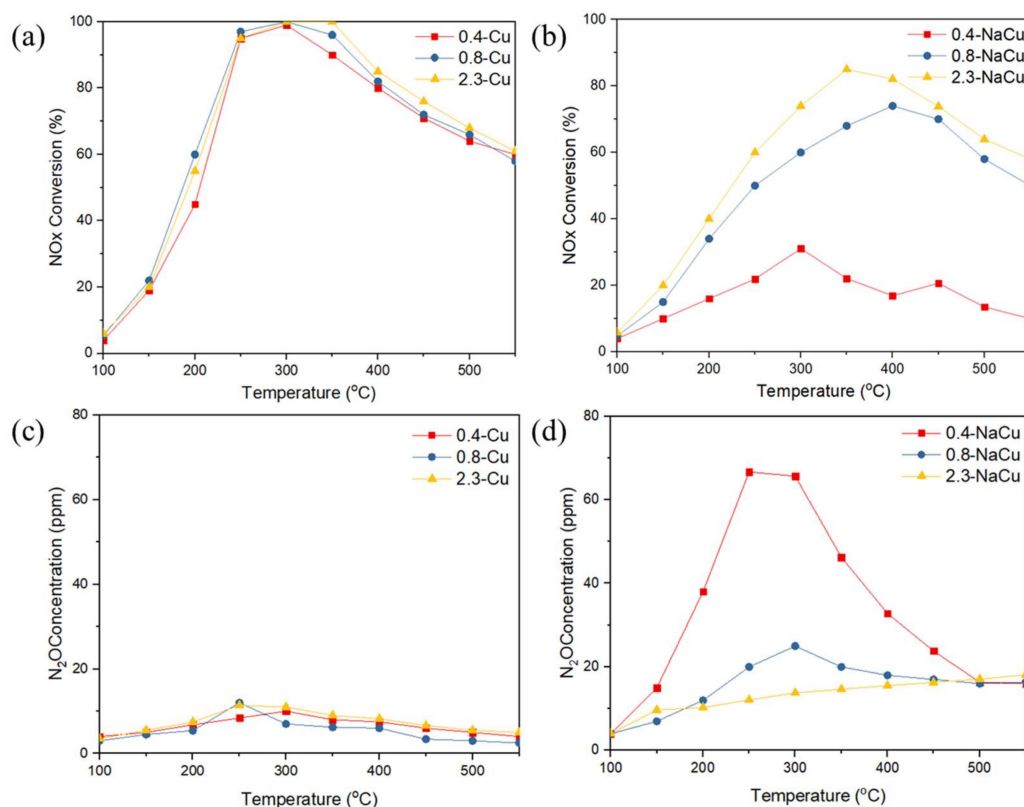


Figure 2. (a,b) NO_x conversion and (c,d) N₂O formation of Cu/SSZ-13 before and after Na poisoning. The gas feed contains 500 ppm NO_x, 500 ppm NH₃, 10% O₂, 3% H₂O, balanced N₂. The gas hourly space velocity (GHSV) is 72,000 h⁻¹.

As a side reaction of NH₃-SCR, the NH₃ oxidation reaction was also tested (Figure 3). Before Na poisoning, the NH₃ oxidation performances of 0.4-Cu, 0.8-Cu and 2.3-Cu are almost the same. Temperature-dependent NO_x and N₂O evolutions are recorded as shown in Figure S1. Same trends for all nitrogen oxides are observed. After Na poisoning, the NH₃ oxidation performance of all samples is improved. The active center of NH₃ oxidation can be isolated Cu ions and CuO_x clusters. In the previous report [36], NH₃ oxidation activities on CuO_x clusters are much higher than Cu ions. Therefore, the improvement of NH₃ oxidation is attributed to CuO_x formation in the catalysts. It is noted that 0.4-NaCu has the largest increase in activity, reaching ~100% conversion at 250 °C. In other words, Cu/SSZ-13 with a larger particle size has relatively low ammonia oxidation activity and higher resistance to Na poisoning. This is consistent with the results of NH₃-SCR activity. More importantly, Figure S1 shows that there are two active centers in the oxidation process of NH₃ with temperature ramping. One active center is responsible for the formation of nitrogen oxides at 200–350 °C, and the other is responsible for above 350 °C. This trend of change is likely to be related to the migration of Cu with increasing temperature. As the crystal size increases, the former active center (might be Cu^{II}(NH₃)_n(H₂O)_m [37]) gradually decreases. 2.3-NaCu can hardly see the NO_x volcanic curve around 300 °C. This observation will be further discussed later.

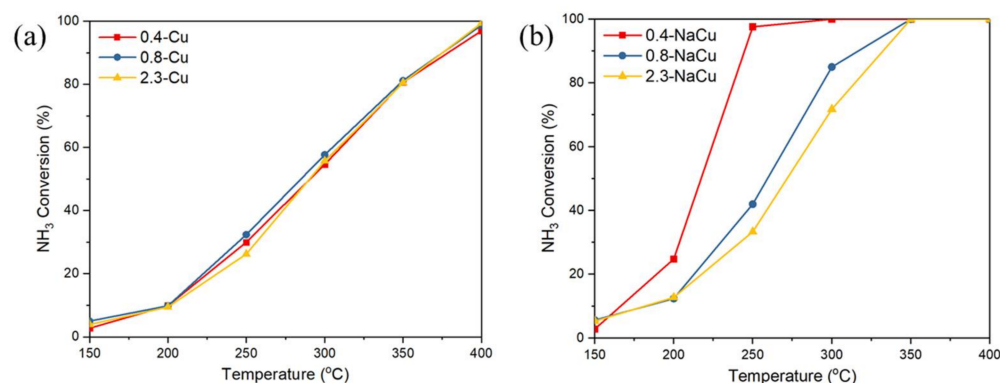


Figure 3. NH₃ oxidation activity of Cu/SSZ-13 (a) before and (b) after Na poisoning. The gas feed contains 500 ppm NH₃, 10% O₂ and balanced N₂. The gas hourly space velocity (GHSV) is 72,000 h⁻¹.

Combined with the results of NH₃-SCR activities, it is interesting to find that Na poisoned Cu/SSZ-13 with a smaller crystal size has a more serious decline in SCR activity and N₂ selectivity. Such reaction trend cannot be separable from the structure of the catalysts caused by different crystal growth paths. Therefore, the characterization of the texture properties and the active center were conducted.

2.2. Texture Properties

The crystal structure was characterized by X-ray diffraction experiments. All catalysts show uniform CHA-type X-ray diffraction patterns (9.7°, 13.1°, 16.3°, 18.0°, 20.9°, 25.4°, 26.3°, 31.1°), as shown in Figure S2. No characteristic peaks corresponding to CuO (35.6°, 38.8°) or Na₂O (36.2°, 46.1°) are observed, which suggests ICP (Table S1) determined ~1.4 wt % Cu and ~2 wt % Na (if Na poisoned) are well dispersed and the particle size of them are under the detection limit. Our previous work reported poisoned Na can induce desilicization and form “H₂Si₂O₅” crystal phase (21.8°) [38]. As shown in Figure 4, it shows that the larger the crystal size of the molecular sieve is, the easier it is to desilicize. However, the structural desilicization occurs on the H/SSZ-13 but not Cu/SSZ-13, which shows that Cu ions play a role in protecting the Si framework. The nature of SSZ-13 determines the acid sites (Si-OH-Al) formation in the zeolites. Na poisoned samples presented the “H₂Si₂O₅” crystal phase (21.8°), which indicates desilicization occurs. When Cu was loaded, such desilicization was much weakened. The results show that

desilicization is likely to happen on the acid sites. Si-O($\text{Cu}^{\text{II}}\text{OH}$)-Al or Al-O- Cu^{II} -O-Si-O-Al sites can be kept after Na poisoning.

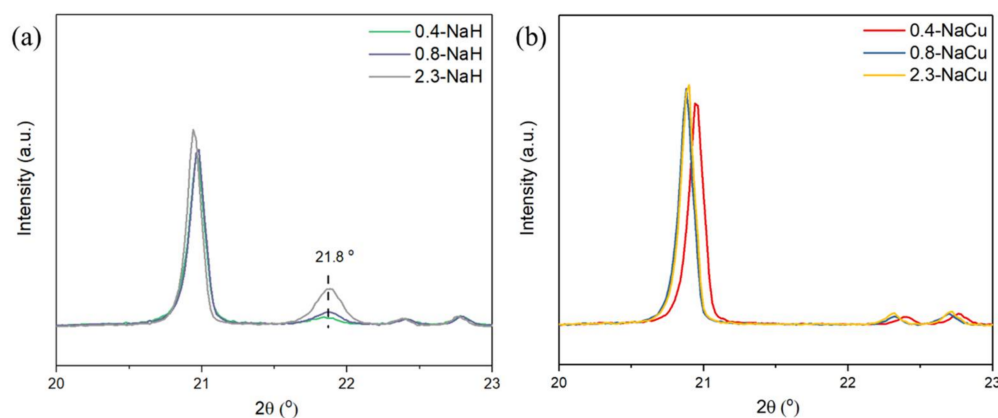


Figure 4. 20–23° XRD patterns of Na-poisoned (a) H/SSZ-13 supports and (b) Cu/SSZ-13 catalysts.

The N_2 adsorption and desorption experiments are used to characterize the pore structure of the catalysts. As shown in Table 1, the BET specific surface area of both SSZ-13 and CuSSZ-13 is greater than $800 \text{ m}^2/\text{g}$. However, the support SSZ-13 is easily damaged by Na poisoning, and the specific surface area is greatly reduced. This is consistent with the XRD results. The desilicization is believed to cause such variation on the specific surface area. In contrast, the tolerance of Cu/SSZ-13 to Na is much improved. The pore distribution was also analyzed and found that the pore structure is rarely damaged by Na poisoning (Figure S3).

Table 1. BET Specific surface area of samples.

Samples	BET Specific Surface Area (m^2/g)	Samples	BET Specific Surface Area (m^2/g)
0.4-H	831	0.4-Cu	820
0.8-H	832	0.8-Cu	807
2.3-H	825	2.3-Cu	843
0.4-NaH	469	0.4-NaCu	795
0.8-NaH	500	0.8-NaCu	772
2.3-NaH	587	2.3-NaCu	833

The framework coordination structure of the catalyst was also characterized by NMR technology. Normalized ^{27}Al and ^{29}Si NMR spectra show that the coordination of Si and Al has little change before and after Na poisoning, independent of the crystal size of Cu/SSZ-13 (Figure S4). All samples present framework tetrahedral Al at 60 ppm. Corresponding feature of Si at -109 , -103 , and -99 ppm are attributed to Si(4Si, 0Al), Si(3Si, 1Al), and Si(2Si, 2Al), respectively.

The results of structural characterizations (XRD, BET, NMR) consistently indicate that even though Na poisoning may destroy the structure of the SSZ-13 supports, the loading of Cu greatly improves the tolerance to Na poisoning. The texture properties of Cu/SSZ-13 with different crystal sizes have little variation between each other.

2.3. Cu Distribution

Figure 5 presents hydrogen temperature-programmed reduction (H_2 -TPR) profiles of CuSSZ-13 catalysts with different crystal sizes before and after Na poisoning. According to previous reports, it is generally believed that the H_2 reduction peak at 200°C and 400°C are attributed to the reduction of the eight-membered ring (8MR) Cu^{2+} ions and six-membered ring (6MR) Cu^{2+} ions to Cu^+ , respectively. The reduction peak above 500°C is the reduction of Cu^+ to Cu^0 [12,39]. As shown in Figure 5a, an H_2 reduction peak

dominates at ~ 181 °C, while the one at ~ 400 °C is not significant. For Cu/SSZ-13 with Si/Al of ~ 25 , Cu^{2+} is mostly in the form of $\text{Z}[\text{Cu}^{\text{II}}\text{OH}]$ (Z represents the negatively charged framework site), rather than $\text{Z}_2\text{Cu}^{\text{II}}$, because the probability of having two Al atoms in a six-membered ring (6MR) at the same time is relatively small. ^{29}Si NMR results also show that Si (3Si, 1Al) species dominate the framework structure (Figure S4). However, an unexpected result is that the larger the crystal size, the fewer Cu species can be reduced. This is in contradiction with the result that the total Cu content of 0.4-Cu, 0.8-Cu, and 2.3-Cu detected by ICP is 1.05 wt %, 1.38 wt %, and 1.44 wt %, respectively. Note that UV-vis characterization (Figure 6) confirms the ICP results, in which the charge transfer of O^{2-} to Cu^{2+} at 200 nm bands follows an order: 0.4-Cu < 0.8-Cu < 2.3-Cu. Why does the amount of reducible Cu decrease with increasing crystal size? What needs to be certain is that the kinetic radius of H_2 is small enough to pass through the molecular sieve and reach the Cu ion surface. Therefore, it is reasonable to believe that more stable Cu ions in the larger-sized Cu/SSZ-13 make them less reducible. Meanwhile, with the increasing crystal sizes, the shifting to a higher reduction temperature of Cu^+ to Cu^0 is observed. It also indicated that the interaction between Cu ions and supports becomes stronger for the Cu/SSZ-13 with a larger crystal size. After Na poisoning, the reduction peaks shift to lower temperatures, which was previously observed in the literature [13,40]. The peak at 150 °C is attributed to the reduction of $\text{Z}[\text{Cu}^{\text{II}}\text{OH}]$ to Cu^+ , and the sharp one at 220 °C is attributed to the reduction of CuO to Cu^0 . Here we classify the reducing species at ~ 220 °C as CuO, because UV-vis characterizes the formation of a large amount of CuO shown in Figure 6. The amount of produced CuO is proportional to the increase in NH_3 oxidation reaction activity. Besides, the amount of reducible Cu of different samples is still the same as that of fresh samples. The reason why the increase in the particle size leads to the stronger interaction between Cu and the supports is still unclear.

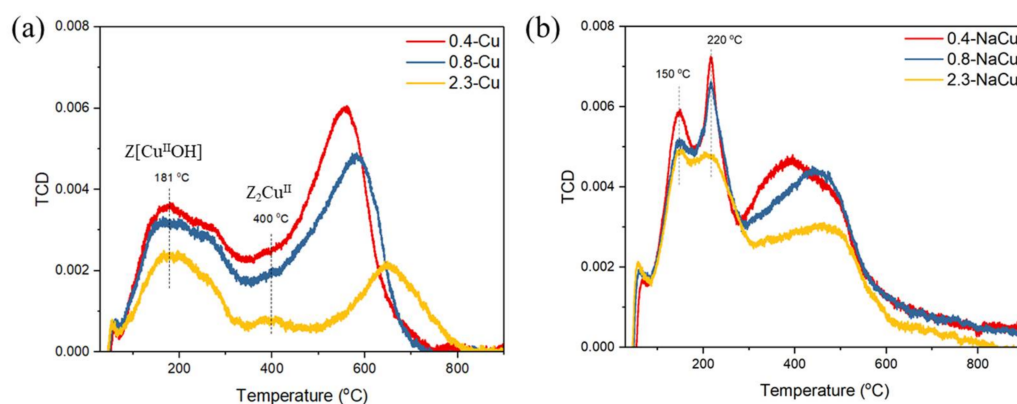


Figure 5. H_2 -TPR profiles of Cu/SSZ-13 with different crystal sizes (a) before and (b) after Na poisoning.

2.4. Acidic Distribution

In the beginning, the target of designing the Cu/SSZ-13 with different crystal sizes is to tune the surface acid sites. The spatial acidic distribution of Cu/SSZ-13 was revealed by comparing the surface acid sites and bulky acid sites. Figure S5 shows the ammonia temperature-programmed desorption (NH_3 -TPD) profiles. NH_3 molecules are small enough to penetrate the SSZ-13 zeolites and therefore can be used to characterize the bulky acid sites. The results show that Cu/SSZ-13 catalysts with different crystal sizes own a similar amount of bulky acid sites. Even Na-poisoned samples have a similar total acid amount, which is mainly dominated by weakly adsorbed acids.

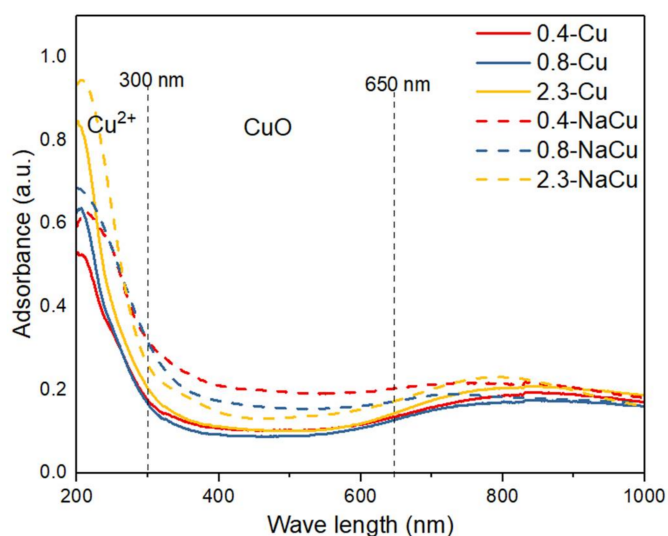


Figure 6. UV-vis spectra of the Cu/SSZ-13 with different crystal sizes.

Diethylamine is a probe molecule often used to investigate the surface acidity of microporous molecular sieves. Its kinetic diameter (4.5 Å) is larger than the pore size of the SSZ-13 molecular sieve (3.8 Å), which ensures that it can only bind to the acidic sites on the outer surface of the crystal. As shown in Figure 7a, only 0.4-Cu sample can adsorb diethylamine molecules. The results of diethylamine TPD for H/SSZ-13 catalysts in Figure 7c show that the smaller the crystal size, the more surface acid sites. It can be inferred that Cu is more present on the surface with a small crystal size, and as the crystal size increases, Cu is distributed in the subsurface or core, i.e., little diethylamine adsorption on the surface of 0.8-Na and 2.3-Na. For the Na-poisoned samples, two desorption peaks of diethylamine can be observed at ~200 °C and 300 °C in Figure 7b,d. Comparing the results of H/SSZ-13 and NaH/SSZ-13, it can be found that partial Na ions can substitute Brønsted acid sites and adsorb diethylamine on the surface of the molecular sieve. It is reasonable that there is almost no diethylamine adsorbing on the 2.3-NaH, because its surface acid sites are limited. Besides, with the decrease of the crystal size and the more acid sites on the surface, replaced Na ions remains on the outer surface. The acidic characteristics of the outer surface of Na-poisoned Cu/SSZ-13 are also in line with expectations. The Na substitution of Cu and the formation of CuO clusters are the basic characteristic of CuSSZ-13 alkali metal poisoning [25]. The newly generated acid sites on the outer surface of 0.8-Na and 2.3-Na are attributed to the formation of CuO clusters, which is consistent with the trends of CuO determined by UV-vis and ammonia oxidation activity.

The acidity of the outer surface of the catalyst was also quantitatively tested by pyridine infrared technology. Pyridine is a molecule with a larger kinetic radius of 5.7 Å, which can only interact with the acid sites on the outer surface of Cu/SSZ-13. According to previous studies [41–43], The IR bands at 1450 and 1593 cm^{-1} are attributed to the chemisorbed pyridine on the Lewis acid sites of the zeolites. The IR band at 1483 cm^{-1} is assigned to the pyridine bonded on both Lewis and Brønsted acid sites. The IR band at 1630 cm^{-1} is attributed to the Brønsted acid sites. As shown in Figure 8, the results show that the smaller the crystal size is, the more Brønsted acid and Lewis acid are on the surface. Although there is a certain deviation on surface quantification from the diethylamine-TPD, the trend is highly consistent.

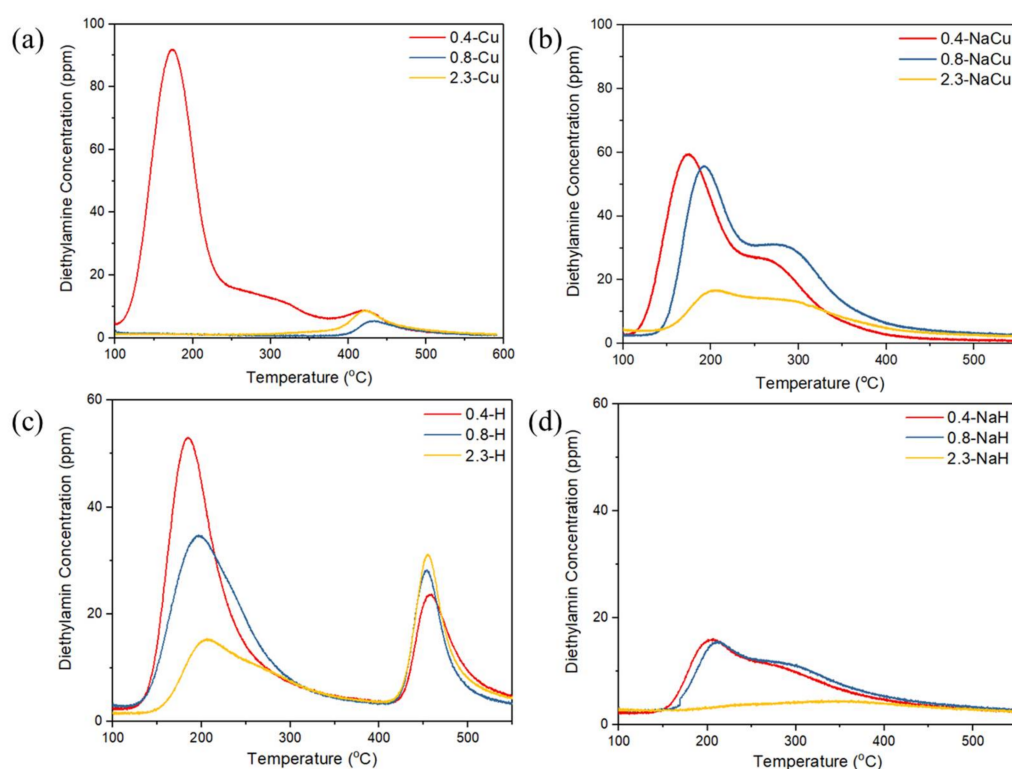


Figure 7. Diethylamine-TPD profiles of Cu/SSZ-13 (a,b) and H/SSZ-13 (c,d) before and after Na poisoning.

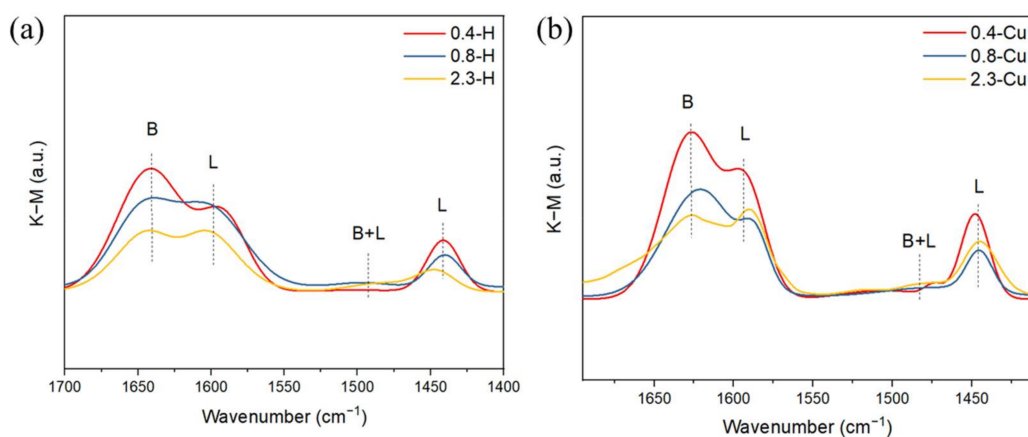


Figure 8. Pyridine-chemisorbed IR spectra of (a) H/SSZ-13 and (b) Cu/SSZ-13 with different crystal sizes before Na poisoning.

In addition to chemical adsorption methods, we expect to visually investigate the spatial distribution of Cu ions on SSZ-13. Combined with cross-section polishing technology, the Cu/SSZ-13 is cut and the Cu content is analyzed by EDS. As shown in Figure 9, point EDS analysis was conducted from the center to the edge of the Cu/SSZ-13 cross-section for four individual crystals. The detected Cu content is summarized in Table 2. The energy spectra are attached to the supporting information (Figure S6). The results show that the distribution of Cu in the molecular sieve forms a decreasing gradient from the center to the edge. Note that it is hard to detect Cu on the surface and subsurface. Such a feature provides sufficient outer surface space to buffer the corrosion of Na, thereby protecting the Cu ions in the core.

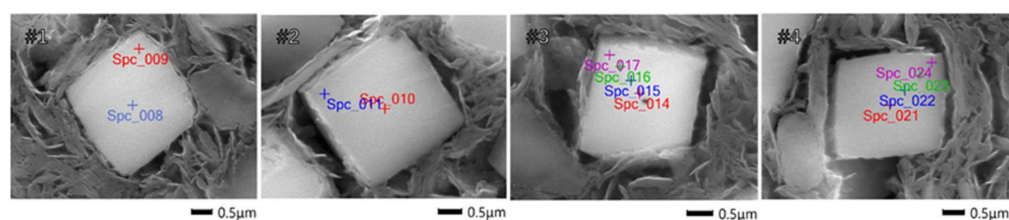


Figure 9. Point EDS analysis of 2.3-Cu sample.

Table 2. Cu content of 2.3-Cu cross-section from the center to the edge.

Detecting Number	Cu Content from Center to Edge/wt %
#1	0.87 ± 0.06, 0.10 ± 0.03
#2	0.76 ± 0.07, 0.08 ± 0.04
#3	0.80 ± 0.03, 0.62 ± 0.06, 0.21 ± 0.02, 0.09 ± 0.02
#4	0.67 ± 0.04, 0.55 ± 0.06, 0.32 ± 0.03, 0.09 ± 0.03

It is time to recall the changes in NH_3 oxidation performance of Cu/SSZ-13 with different crystal sizes before and after Na poisoning. According to our analysis, the side reaction of NH_3 oxidation of Na-poisoned Cu/SSZ-13 with larger crystal size is not significantly improved (Figure 3), and the number of active centers around 300 °C decreases with the increase of crystal sizes (Figure S1). This is rationalized by the difference in spatial acidity distribution. On the one hand, the smaller the crystal size, the more acidic the surface of Cu/SSZ-13 is, and the proportion of Cu ions on the surface is greater. This results in the surface Cu ions being susceptible to the Na corrosion to generate CuO species. On the other hand, the Cu ions distributed in the large crystal-sized molecular sieve have extremely strong stability. The interaction between Cu and framework O can be characterized by H_2 -TPR. Because the interaction of Cu and O reflects how difficult the Cu^{2+} can be reduced (or O^{2-} can be split). From the H_2 -TPR results, with increasing crystal sizes more Cu interacts with the framework O so strongly that it cannot be reduced by H_2 . The chemical bond between the core Cu ions and framework O might be strong enough that NH_3 or H_2O cannot solvate Cu ions, which explains why the $\text{Cu}^{\text{II}}(\text{NH}_3)_n(\text{H}_2\text{O})_m$ species are less distributed in the large-sized Cu/SSZ-13. This inference is based on the fact that the active center of NH_3 oxidation will change with increasing temperature. Chemically, isolated Cu (II) in the six-member ring of SSZ-13 is the active center. It can be solvated by H_2O and NH_3 molecules to form so-called hydrated or ammoniated Cu (II) species ($\text{Cu}^{\text{II}}(\text{NH}_3)_n(\text{H}_2\text{O})_m$). Gao et al. reported that the activation energy of Cu/SSZ-13 in the low-temperature region (200–260 °C) and the high-temperature region (400–460 °C) of the NH_3 oxidation reaction are 64.1 kJ/mol and 150 kJ/mol, respectively [39]. Therefore, it is reasonable to believe that the reaction path is different in the two different temperature ranges, and the active center transforms from solvable $\text{Cu}^{\text{II}}(\text{NH}_3)_n(\text{H}_2\text{O})_m$ to framework-anchored $\text{ZCu}^{\text{II}}\text{OH}$ as the temperature crosses ~300 °C.

3. Materials and Methods

3.1. Catalysts Preparation

Na/SSZ-13 (Si/Al = 25) was home-made according to previous reports [2,44,45]. The crystal size of SSZ-13 was controlled by adding different amounts of seed crystals [46]. During the hydrothermal synthesis process, other conditions remain the same, such as crystallization temperature (160 °C), crystallization time (72 h), silicon source (silica sol, Jiyida Co. Ltd., Qingdao, China), aluminum source (pseudo-boehmite, Chinalco, Zibo, China), template agent (1-Adamantanamine, Sigma-Aldrich, Beijing, China), etc. The templating agent was removed from as-prepared Na/SSZ-13 by calcinating at 650 °C for 4 h. Cu/SSZ-13 was obtained by the aqueous ion-exchange method. Briefly, following Na/SSZ-13 with the template removed, NH_4 /SSZ-13 was obtained by twice ion-exchanging with 0.1M NH_4NO_3 . Then NH_4 /SSZ-13 was ion-exchanged by 0.1M $\text{Cu}(\text{NO}_3)_2$ to prepare

Cu/SSZ-13. H/SSZ-13 was also prepared by calcinating $\text{NH}_4/\text{SSZ-13}$ at $550\text{ }^\circ\text{C}$ for 4 h. The samples were denoted by 'x-Cu' and 'x-H' to respectively represent Cu/SSZ-13 catalysts and H/SSZ-13 supports with different crystal sizes, where x is the crystal size (μm).

To simulate the alkali metal poisoning process, a combination of equal volume impregnation and high-temperature hydrothermal aging was carried out. In detail, it was impregnated with NaNO_3 on the samples and aged for 12 h at $600\text{ }^\circ\text{C}$ under 10 vol % steam. 'x-NaCu' and 'x-NaH' were used to represent Na-poisoned samples.

3.2. Characterization

The morphology of the sample was pictured on a field emission electron microscopy (Regulus 8100, HITACHI, Tokyo, Japan) at 3 kV.

The powder X-ray diffraction (XRD) patterns of the catalysts were detected using a Rigaku Smartlab XRD (Tokyo, Japan) with Cu $K\alpha$ radiation source. The X-ray emission tube was run at 40 kV and 40 mA. The diffraction angle (2θ) range of $5\text{--}50^\circ$ was chosen to identify the crystal phases.

The BET surface area was measured with a physisorption analyzer (ASAP 2460, Micromeritics) at 77K. Before testing, the samples were vacuumed under $300\text{ }^\circ\text{C}$ for 3 h.

The NMR spectra were recorded using a JEOL JNM-ECZ600R spectrometer (Tokyo, Japan). The ^{29}Si and ^{27}Al NMR were carried out at a field strength of 14.1 T with a total scanning of 1200 and 300 times, relaxation delay of 10s and 2s, respectively. The tube diameter of 4 mm and 8 mm was chosen for testing ^{27}Al and ^{29}Si , respectively.

Hydrogen temperature-programmed reduction (H_2 -TPR) was carried out in a Micromeritics AutoChem 2920 II system (Micromeritics). The catalysts were pretreated under 5% O_2/N_2 at $500\text{ }^\circ\text{C}$ for 30 min. The H_2 -TPR profile was recorded from ambient to $900\text{ }^\circ\text{C}$ at a rate of $10\text{ }^\circ\text{C}/\text{min}$.

UV-vis spectra were collected in a SHIMADZU UV-2600 (Kyoto, Japan) equipped with an integrating sphere assembly. The sample powder was pressed into a cake in the button groove at ambient. A pressed cake of BaSO_4 was used as the reference.

Diethylamine temperature-programmed desorption measurement was conducted using a plug flow microreactor. The diethylamine was detected using an online Fourier transmission infrared spectrometer (MultiGas 6030, MKS). The sample was pretreated under 5% O_2/N_2 at $500\text{ }^\circ\text{C}$ for 30 min, followed by diethylamine saturation at $100\text{ }^\circ\text{C}$. The weakly adsorbed diethylamine was purged by N_2 and then the sample was heated to $550\text{ }^\circ\text{C}$ at a rate of $10\text{ }^\circ\text{C}/\text{min}$.

Operando pyridine titration experiment was monitored by a diffuse reflection infrared Fourier transform spectrometer (DRIFTS) (Nicolet 6700, Thermo). The sample was pretreated at $500\text{ }^\circ\text{C}$ for 30 min under 5% O_2/N_2 . Then it was cooled to $250\text{ }^\circ\text{C}$ under N_2 and the background spectrum was collected. The in-situ time-resolved spectra were recorded when the N_2 carrier with pyridine mixed gas pass through the sample.

3.3. Catalytic Evaluation

The standard NH_3 -SCR activity was tested with a plug flow microreactor. The powder sample was supported by quartz wool on both sides. Typically, 0.1 g catalyst was mixed with 0.9 g quartz sand to uniformly disperse catalysts powder. The simulated gas contains 500 ppm NH_3 , 500 ppm NO , 10% O_2 , 3% H_2O and balanced N_2 . The gas hourly space velocity (GHSV) is $72,000\text{ h}^{-1}$. The NO_x conversion was calculated as below,

$$\text{NO}_x\ \% = \frac{[\text{NO}_x]_{\text{in}} - [\text{NO}_x]_{\text{out}}}{[\text{NO}_x]_{\text{in}}} \times 100\% \quad (1)$$

The NH₃ oxidation activity was also investigated individually. The experiment setup is the same as that for the NH₃-SCR activity measurement. 500 ppm NH₃, 10% O₂ and balanced N₂ were used. The NH₃ conversion was calculated as below,

$$\text{NH}_3 \% = \frac{[\text{NH}_3]_{\text{in}} - [\text{NH}_3]_{\text{out}}}{[\text{NH}_3]_{\text{in}}} \times 100\% \quad (2)$$

The reagents and products were monitored by an online FTIR spectrometer (Multigas 6030, MKS). For each sample, the activity test included pre-treatment and steady-state activity testing. For example, the catalysts were firstly oxidized under 10% O₂/N₂ at 500 °C for 1 h. The ready catalyst was then fed with mixed gases of standard NH₃-SCR or NH₃ oxidation. The steady-state data were collected from 500 °C to 100 °C in an interval of 50 °C.

4. Conclusions

Cu/SSZ-13 catalysts with similar Cu loadings and different crystal sizes (0.4–2.3 μm) were controllably synthesized. Although the pore structure of H/SSZ-13 with a large crystal size is susceptible to Na poisoning, the loading of Cu ions has a strong protective effect on the structure. It was found that increasing the crystal size of Cu/SSZ-13 catalysts can effectively improve the Na resistance. Large crystal size is conducive to the distribution of acidic sites on the subsurface or inner core of the molecular sieve. The Cu ions distributed in the deep layer have strong redox stability and are not easily solvated by NH₃ or H₂O molecules. The richer Cu ions on the outer surface of Cu/SSZ-13 with smaller particle size is more susceptible to Na ion exchange to generate more CuO species. The decrease of Cu ions and the increase of CuO clusters are the main reasons for the decrease of NH₃-SCR activity and the increase of side reaction NH₃ oxidation activity. The results are helpful to guide industrial applications in heavy-duty diesel engines after treatment by improving the alkali metal tolerance of commercial Cu/SSZ-13 catalysts for NH₃-SCR reaction.

Supplementary Materials: The following are available online at <https://www.mdpi.com/article/10.3390/catal11080979/s1>, Figure S1: NO_x and N₂O concentration evolution in the NH₃ oxidation; Figure S2. XRD patterns of Cu/SSZ-13 (a) before and (b) after Na poisoning; Figure S3. The micropore distribution of Cu/SSZ-13 (a) before and (b) after Na poisoning; Figure S4. (a–b) ²⁷Al NMR spectra and (c–d) ²⁹Si NMR spectra of CuSSZ-13 before and after Na poisoning; Figure S5. NH₃-TPD profiles of Cu/SSZ-13 with different crystal sizes (a) before and (b) after Na poisoning; Figure S6. Point EDS spectra corresponding to the results in Figure 9, Table S1. Element composition of Cu/SSZ-13 and Na-poisoned counterparts with different crystal sizes.

Author Contributions: Conceptualization, Z.C. and M.S.; Methodology, C.W.; Validation, Z.C., J.W. (Jianqiang Wang), and J.W. (Jun Wang); Formal analysis, Z.C.; Investigation, Z.C.; Writing—original draft preparation, Z.C.; Writing—review and editing, J.W. (Jianqiang Wang) and C.W.; Supervision, M.S. and G.S.; Project administration, J.W. (Jun Wang) and G.S.; Funding acquisition, J.W. (Jun Wang). All authors have read and agreed to the published version of the manuscript.

Funding: This research was funded by Foundation for Innovative Research Groups of the National Natural Science Foundation of China, grant number 51921004; Major Science and Technology Programs of Yunnan, grant number 202002AB080001-1; National Natural Science Foundation for Youth of China, grant number 21908207 and Postdoctoral Research Foundation of China, grant number 2020M670659; Shanxi Province Science Foundation for Youths, grant number 201901D211224.

Acknowledgments: We are grateful to all our funders.

Conflicts of Interest: The authors declare no conflict of interest.

References

1. Joshi, A. Review of Vehicle Engine Efficiency and Emissions. *SAE Tech. Pap.* **2021**. [CrossRef]
2. Kwak, J.H.; Tonkyn, R.G.; Kim, D.H.; Szanyi, J.; Peden, C.H.F. Excellent activity and selectivity of Cu-SSZ-13 in the selective catalytic reduction of NO_x with NH₃. *J. Catal.* **2010**, *275*, 187–190. [CrossRef]
3. Ma, L.; Cheng, Y.; Cavataio, G.; McCabe, R.W.; Fu, L.; Li, J. Characterization of commercial Cu-SSZ-13 and Cu-SAPO-34 catalysts with hydrothermal treatment for NH₃-SCR of NO_x in diesel exhaust. *Chem. Eng. J.* **2013**, *225*, 323–330. [CrossRef]

4. Fan, C.; Chen, Z.; Pang, L.; Ming, S.; Dong, C.; Brou Albert, K.; Liu, P.; Wang, J.; Zhu, D.; Chen, H.; et al. Steam and alkali resistant Cu-SSZ-13 catalyst for the selective catalytic reduction of NO_x in diesel exhaust. *Chem. Eng. J.* **2018**, *334*, 344–354. [[CrossRef](#)]
5. Jiang, H.; Guan, B.; Peng, X.; Zhan, R.; Lin, H.; Huang, Z. Influence of synthesis method on catalytic properties and hydrothermal stability of Cu/SSZ-13 for NH₃-SCR reaction. *Chem. Eng. J.* **2020**, *379*, 122358. [[CrossRef](#)]
6. Wang, J.; Peng, Z.; Chen, Y.; Bao, W.; Chang, L.; Feng, G. In-situ hydrothermal synthesis of Cu-SSZ-13/cordierite for the catalytic removal of NO_x from diesel vehicles by NH₃. *Chem. Eng. J.* **2015**, *263*, 9–19. [[CrossRef](#)]
7. Lomachenko, K.A.; Borfecchia, E.; Negri, C.; Berlier, G.; Lamberti, C.; Beato, P.; Falsig, H.; Bordiga, S. The Cu-CHA deNO_x Catalyst in Action: Temperature-Dependent NH₃-Assisted Selective Catalytic Reduction Monitored by Operando XAS and XES. *J. Am. Chem. Soc.* **2016**, *138*, 12025–12028. [[CrossRef](#)] [[PubMed](#)]
8. Janssens, T.V.W.; Falsig, H.; Lundegaard, L.F.; Vennestrom, P.N.R.; Rasmussen, S.B.; Moses, P.G.; Giordanino, F.; Borfecchia, E.; Lomachenko, K.A.; Lamberti, C.; et al. A Consistent Reaction Scheme for the Selective Catalytic Reduction of Nitrogen Oxides with Ammonia. *ACS Catal.* **2015**, *5*, 2832–2845. [[CrossRef](#)]
9. Bates, S.A.; Verma, A.A.; Paolucci, C.; Parekh, A.A.; Anggara, T.; Yezerets, A.; Schneider, W.F.; Miller, J.T.; Delgass, W.N.; Ribeiro, F.H. Identification of the active Cu site in standard selective catalytic reduction with ammonia on Cu-SSZ-13. *J. Catal.* **2014**, *312*, 87–97. [[CrossRef](#)]
10. Gunter, T.; Carvalho, H.W.; Doronkin, D.E.; Sheppard, T.; Glatzel, P.; Atkins, A.J.; Rudolph, J.; Jacob, C.R.; Casapu, M.; Grunwaldt, J.D. Structural snapshots of the SCR reaction mechanism on Cu-SSZ-13. *Chem. Commun.* **2015**, *51*, 9227–9230. [[CrossRef](#)] [[PubMed](#)]
11. Paolucci, C.; Khurana, I.; Parekh, A.A.; Li, S.; Shih, A.J.; Li, H.; Di Iorio, J.R.; Albarracin-Caballero, J.D.; Yezerets, A.; Miller, J.T.; et al. Dynamic multinuclear sites formed by mobilized copper ions in NO_x selective catalytic reduction. *Science* **2017**, *357*, 898–903. [[CrossRef](#)] [[PubMed](#)]
12. Hun Kwak, J.; Zhu, H.; Lee, J.H.; Peden, C.H.; Szanyi, J. Two different cationic positions in Cu-SSZ-13? *Chem. Commun.* **2012**, *48*, 4758–4760. [[CrossRef](#)] [[PubMed](#)]
13. Cui, Y.; Wang, Y.; Mei, D.; Walter, E.D.; Washton, N.M.; Holladay, J.D.; Wang, Y.; Szanyi, J.; Peden, C.H.F.; Gao, F. Revisiting effects of alkali metal and alkaline earth co-cation additives to Cu/SSZ-13 selective catalytic reduction catalysts. *J. Catal.* **2019**, *378*, 363–375. [[CrossRef](#)]
14. Jiang, H.; Guan, B.; Peng, X.; Wei, Y.; Zhan, R.; Lin, H.; Huang, Z. Effect of sulfur poisoning on the performance and active sites of Cu/SSZ-13 catalyst. *Chem. Eng. Sci.* **2020**, *226*, 115855. [[CrossRef](#)]
15. Olsson, L.; Wijayanti, K.; Leistner, K.; Kumar, A.; Joshi, S.Y.; Kamasamudram, K.; Currier, N.W.; Yezerets, A. A kinetic model for sulfur poisoning and regeneration of Cu/SSZ-13 used for NH₃-SCR. *Appl. Catal. B Environ.* **2016**, *183*, 394–406. [[CrossRef](#)]
16. Gao, F.; Wang, Y.; Washton, N.M.; Kollár, M.; Szanyi, J.; Peden, C.H.F. Effects of Alkali and Alkaline Earth Cocations on the Activity and Hydrothermal Stability of Cu/SSZ-13 NH₃-SCR Catalysts. *ACS Catal.* **2015**, *5*, 6780–6791. [[CrossRef](#)]
17. Deka, U.; Lezcano-Gonzalez, I.; Weckhuysen, B.M.; Beale, A.M. Local Environment and Nature of Cu Active Sites in Zeolite-Based Catalysts for the Selective Catalytic Reduction of NO_x. *ACS Catal.* **2013**, *3*, 413–427. [[CrossRef](#)]
18. Jangjou, Y.; Do, Q.; Gu, Y.; Lim, L.-G.; Sun, H.; Wang, D.; Kumar, A.; Li, J.; Grabow, L.C.; Epling, W.S. Nature of Cu Active Centers in Cu-SSZ-13 and Their Responses to SO₂ Exposure. *ACS Catal.* **2018**, *8*, 1325–1337. [[CrossRef](#)]
19. Song, J.; Wang, Y.; Walter, E.D.; Washton, N.M.; Mei, D.; Kovarik, L.; Engelhard, M.H.; Proding, S.; Wang, Y.; Peden, C.H.F.; et al. Toward Rational Design of Cu/SSZ-13 Selective Catalytic Reduction Catalysts: Implications from Atomic-Level Understanding of Hydrothermal Stability. *ACS Catal.* **2017**, *7*, 8214–8227. [[CrossRef](#)]
20. Lin, C.; Cao, Y.; Feng, X.; Lin, Q.; Xu, H.; Chen, Y. Effect of Si islands on low-temperature hydrothermal stability of Cu/SAPO-34 catalyst for NH₃-SCR. *J. Taiwan Inst. Chem. Eng.* **2017**, *81*, 288–294. [[CrossRef](#)]
21. Schwab, S.D.; Bennett, J.J.; Dell, S.J.; Galante-Fox, J.M.; Kulinoski, A.M.; Miller, K.T. Internal Injector Deposits in High-Pressure Common Rail Diesel Engines. *SAE Int. J. Fuels Lubr.* **2010**, *3*, 865–878. [[CrossRef](#)]
22. Liu, L.; Wu, X.; Ma, Y.; Zhang, X.; Ran, R.; Si, Z.; Weng, D. Potassium deactivation of Cu-SSZ-13 catalyst for NH₃-SCR: Evolution of salts, zeolite and copper species. *Chem. Eng. J.* **2020**, *383*, 123080. [[CrossRef](#)]
23. Williams, A.; McCormick, R.; Lance, M.; Xie, C.; Toops, T.; Brezny, R. Effect of Accelerated Aging Rate on the Capture of Fuel-Borne Metal Impurities by Emissions Control Devices. *SAE Int. J. Fuels Lubr.* **2014**, *7*, 471–479. [[CrossRef](#)]
24. Williams, A.; Burton, J.; McCormick, R.L.; Toops, T.; Wereszczak, A.A.; Fox, E.E.; Lance, M.J.; Cavataio, G.; Dobson, D.; Warner, J.; et al. Impact of Fuel Metal Impurities on the Durability of a Light-Duty Diesel Aftertreatment System. *SAE Tech. Pap.* **2013**. [[CrossRef](#)]
25. Wang, C.; Yan, W.; Wang, Z.; Chen, Z.; Wang, J.; Wang, J.; Wang, J.; Shen, M.; Kang, X. The role of alkali metal ions on hydrothermal stability of Cu/SSZ-13 NH₃-SCR catalysts. *Catal. Today* **2020**, *355*, 482–492. [[CrossRef](#)]
26. Wang, C.; Wang, C.; Wang, J.; Wang, J.; Shen, M.; Li, W. Effects of Na(+) on Cu/SAPO-34 for ammonia selective catalytic reduction. *J. Environ. Sci.* **2018**, *70*, 20–28. [[CrossRef](#)] [[PubMed](#)]
27. Yan, Q.; Nie, Y.; Yang, R.; Cui, Y.; O'Hare, D.; Wang, Q. Highly dispersed Cu_yAlO_x mixed oxides as superior low-temperature alkali metal and SO₂ resistant NH₃-SCR catalysts. *Appl. Catal. A Gen.* **2017**, *538*, 37–50. [[CrossRef](#)]
28. Liu, A.; Liu, L.; Cao, Y.; Wang, J.; Si, R.; Gao, F.; Dong, L. Controlling Dynamic Structural Transformation of Atomically Dispersed CuO_x Species and Influence on Their Catalytic Performances. *ACS Catal.* **2019**, *9*, 9840–9851. [[CrossRef](#)]

29. Du, Y.; Huang, Z.; Zhang, J.; Jing, G. Fe₂O₃/HY Catalyst: A Microporous Material with Zeolite-Type Framework Achieving Highly Improved Alkali Poisoning-Resistant Performance for Selective Reduction of NO_x with NH₃. *Environ. Sci. Technol.* **2020**, *54*, 7078–7087. [[CrossRef](#)] [[PubMed](#)]
30. Zha, K.; Kang, L.; Feng, C.; Han, L.; Li, H.; Yan, T.; Maitarad, P.; Shi, L.; Zhang, D. Improved NO_x reduction in the presence of alkali metals by using hollandite Mn–Ti oxide promoted Cu-SAPO-34 catalysts. *Environ. Sci. Nano.* **2018**, *5*, 1408–1419. [[CrossRef](#)]
31. Huang, S.; Wang, J.; Wang, J.; Wang, C.; Shen, M.; Li, W. The influence of crystallite size on the structural stability of Cu/SAPO-34 catalysts. *Appl. Catal. B Environ.* **2019**, *248*, 430–440. [[CrossRef](#)]
32. Kumar, M.; Luo, H.; Román-Leshkov, Y.; Rimer, J.D. SSZ-13 Crystallization by Particle Attachment and Deterministic Pathways to Crystal Size Control. *J. Am. Chem. Soc.* **2015**, *137*, 13007–13017. [[CrossRef](#)]
33. Gao, F.; Walter, E.D.; Kollar, M.; Wang, Y.; Szanyi, J.; Peden, C.H.F. Understanding ammonia selective catalytic reduction kinetics over Cu/SSZ-13 from motion of the Cu ions. *J. Catal.* **2014**, *319*, 1–14. [[CrossRef](#)]
34. Marberger, A.; Petrov, A.W.; Steiger, P.; Elsener, M.; Kröcher, O.; Nachtegaal, M.; Ferri, D. Time-resolved copper speciation during selective catalytic reduction of NO on Cu-SSZ-13. *Nat. Catal.* **2018**, *1*, 221–227. [[CrossRef](#)]
35. Gao, F.; Mei, D.; Wang, Y.; Szanyi, J.; Peden, C.H.F. Selective Catalytic Reduction over Cu/SSZ-13: Linking Homo- and Heterogeneous Catalysis. *J. Am. Chem. Soc.* **2017**, *139*, 4935–4942. [[CrossRef](#)] [[PubMed](#)]
36. Gao, F.; Kwak, J.H.; Szanyi, J.; Peden, C.H.F. Current Understanding of Cu-Exchanged Chabazite Molecular Sieves for Use as Commercial Diesel Engine DeNO_x Catalysts. *Top. Catal.* **2013**, *56*, 1441–1459. [[CrossRef](#)]
37. Paolucci, C.; Parekh, A.A.; Khurana, I.; Di Iorio, J.R.; Li, H.; Albarracin Caballero, J.D.; Shih, A.J.; Anggara, T.; Delgass, W.N.; Miller, J.T.; et al. Catalysis in a Cage: Condition-Dependent Speciation and Dynamics of Exchanged Cu Cations in SSZ-13 Zeolites. *J. Am. Chem. Soc.* **2016**, *138*, 6028–6048. [[CrossRef](#)]
38. Chen, Z.; Wang, J.; Wang, J.; Wang, C.; Wang, J.; Li, W.; Shen, M. Disparate Essences of Residual, Ion-Exchanged, and Impregnated Na Ions on Topology Structure for Cu/SSZ-13 NH₃ Selective Catalytic Reduction Catalysts. *Ind. Eng. Chem. Res.* **2019**, *58*, 20610–20619. [[CrossRef](#)]
39. Gao, F.; Washton, N.M.; Wang, Y.; Kollár, M.; Szanyi, J.; Peden, C.H.F. Effects of Si/Al ratio on Cu/SSZ-13 NH₃-SCR catalysts: Implications for the active Cu species and the roles of Brønsted acidity. *J. Catal.* **2015**, *331*, 25–38. [[CrossRef](#)]
40. Zhao, Z.; Yu, R.; Zhao, R.; Shi, C.; Gies, H.; Xiao, F.-S.; De Vos, D.; Yokoi, T.; Bao, X.; Kolb, U.; et al. Cu-exchanged Al-rich SSZ-13 zeolite from organotemplate-free synthesis as NH₃-SCR catalyst: Effects of Na⁺ ions on the activity and hydrothermal stability. *Appl. Catal. B Environ.* **2017**, *217*, 421–428. [[CrossRef](#)]
41. Wang, B.; Ma, L.; Han, L.; Feng, Y.; Hu, J.; Xie, W.; Bao, W.; Chang, L.; Huang, Z.; Wang, J. Assembly-reassembly of coal fly ash into Cu-SSZ-13 zeolite for NH₃-SCR of NO via interzeolite transformations. *Chem. Eng. Sci. X* **2021**, *10*, 100089.
42. Fan, J.; Ning, P.; Wang, Y.; Song, Z.; Liu, X.; Wang, H.; Wang, J.; Wang, L.; Zhang, Q. Significant promoting effect of Ce or La on the hydrothermal stability of Cu-SAPO-34 catalyst for NH₃-SCR reaction. *Chem. Eng. J.* **2019**, *369*, 908–919. [[CrossRef](#)]
43. Zhan, H.; Huang, S.; Li, Y.; Lv, J.; Wang, S.; Ma, X. Elucidating the nature and role of Cu species in enhanced catalytic carbonylation of dimethyl ether over Cu/H-MOR. *Catal. Sci. Technol.* **2015**, *5*, 4378–4389. [[CrossRef](#)]
44. Zones, S.I. Zeolite SSZ-13 and Its Method of Preparation. U.S. 4544538A, 1 October 1985.
45. Fickel, D.W.; Lobo, R.F. Copper coordination in Cu-SSZ-13 and Cu-SSZ-16 investigated by variable-temperature XRD. *J. Phys. Chem. C* **2010**, *114*, 1633–1640. [[CrossRef](#)]
46. Wang, J.; Shao, L.; Wang, C.; Wang, J.; Shen, M.; Li, W. Controllable preparation of various crystal size and nature of intracrystalline diffusion in Cu/SSZ-13 NH₃-SCR catalysts. *J. Catal.* **2018**, *367*, 221–228. [[CrossRef](#)]